Article

Journal of
Nanoscience and Nanotechnology
Vol. 18, 4734–4745, 2018
www.aspbs.com/jnn

Catalytic Conversion of Glycerol to Lactic Acid Over Hydroxyapatite-Supported Metallic Ni^0 Nanoparticles

Lang Qiu, Haixu Yin, Hengbo Yin*, and Aili Wang*

Faculty of Chemistry and Chemical Engineering, Jiangsu University, Zhenjiang 212013, China

Catalytic conversion of low-priced biomass glycerol to value-added lactic acid is an alternative route to the conventional fermentation process using sugar as the starting material. Nanosized hydroxyapatite-supported metallic Ni^0 nanoparticles (Ni_x/HAP) prepared by the wetness chemical reduction method effectively catalyzed the conversion of high-concentrated glycerol (1.5–3 mol L^{-1}) to lactic acid in a NaOH aqueous solution. The Ni_x/HAP catalysts exhibited higher catalytic activity for glycerol conversion to lactic acid than the sole metallic Ni^0 nanoparticles. When the reaction was carried out over the $Ni_{0.2}$/HAP catalyst with the initial glycerol and NaOH concentrations of 2.0 and 2.2 mol L^{-1} at 200 °C for 2 h, the selectivity of lactic acid reached 94.7% at the glycerol conversion of 92.1%.

Keywords: Glycerol, Lactic Acid, Hydroxyapatite, Nickel Nanoparticles.

1. INTRODUCTION

To avoid fossil fuel depletion and solve greenhouse gas problem, researchers have made great efforts on the conversion of biomass to biofuel and valuable chemicals.[1–13] Biodiesel, as a renewable and sustainable fuel, produced by transesterification between methanol and vegetable oil or animal fat has been widely used in the world.[4–13] Glycerol, as a by-product, has been produced with ca. 10–20% of the total volume of biodiesel.[14, 15] In 2016, the biodiesel market is estimated to be 37 billion liters. Above 4 billion liters of crude glycerol will be produced, causing an overcapacity problem.[16–18] Therefore, effective conversion of glycerol into high-valued chemicals has attracted great attention of researchers in past decade.[19–22]

Lactic acid can be synthesized using glycerol as a starting material by hydrothermal method in an alkaline solution without or with the use of catalyst, being a potential lactic acid production route to replace the conventional fermentation process using sugar as the starting material.[23–27] The recent research results dealing with the hydrothermal conversion of glycerol to lactic acid are summarized as follows.

Kishida et al. firstly reported that lactic acid with the yield of above 90% was synthesized by the hydrothermal conversion of glycerol (0.33 mol L^{-1}) at 300 °C with the use of NaOH as the homogeneous catalyst in an aqueous solution.[26] Alkali metal hydroxides exhibited higher catalytic activity than alkaline earth metal hydroxides.[18, 23, 26, 27]

To decrease the reaction temperature, heterogeneously catalytic conversion of glycerol to lactic acid has been investigated over supported noble and non-noble metal catalysts. The supported noble metal catalysts, such as Au, Pt, and Pt/Au catalysts could effectively catalyze the aerobic conversion of glycerol to lactic acid in a NaOH aqueous solution at 90–180 °C, giving the lactic acid yield of above 80%.[28–31]

In order to decrease the cost of noble metal for glycerol conversion to lactic acid, copper-based catalysts were investigated to catalyze glycerol conversion to lactic acid in an alkaline solution.[32–34] The copper-based catalysts gave lactic acid yields in the range of 60%–77% after reacting at 240 °C for 6 h.[32] The basic hydroxyapatite- and MgO-supported metallic Cu^0 catalysts gave high lactic acid yields of above 81% after reacting at 230 °C for 2 h.[33, 34] The non-noble metallic Cu^0 catalysts exhibited good catalytic activities for the catalytic conversion of glycerol to lactic acid at a lower reaction temperature than the hydrothermal method with the use of sole NaOH as the catalyst. However, in the above-mentioned processes, the glycerol concentration was generally ca. 1 mol L^{-1} or less. In the viewpoint of economy, catalytic conversion

*Authors to whom correspondence should be addressed.

 1533-4880/2018/18/4734/012 doi:10.1166/jnn.2018.15327

of high-concentrated glycerol to lactic acid is worth of investigation.

Metallic Ni^0 and supported Ni^0 catalysts exhibit good catalytic activities for hydrogenation reactions in industrial processes.[35–39] The nickel-based catalysts should have good dehydrogenation performances according to catalysis principle. Glycerol dehydrogenation is the first step involved in the hydrothermal conversion of glycerol to lactic acid.[33,34] However, to the best of our knowledge, catalytic hydrothermal conversion of glycerol to lactic acid over nickel-based catalysts has not been reported.

In our present work, nanosized hydroxyapatite-supported nickel (Ni_x/HAP) catalysts were investigated to catalyze the hydrothermal conversion of high-concentrated glycerol to lactic acid. The Ni_x/HAP catalysts were prepared by the wetness chemical reduction method and characterized by XRD, TEM, HRTEM, BET, CO_2-TPD, and atomic absorption spectrophotometer techniques. The Ni_x/HAP catalysts effectively catalyzed the conversion of high-concentrated glycerol to lactic acid at a relatively low reaction temperature in a batch reactor.

2. EXPERIMENTAL DETAILS

2.1. Materials

Ammonia solution (25%), phosphoric acid (85%), calcium nitrate tetrahydrate, anhydrous ethanol, sodium hydroxide, nickel acetate tetrahydrate ($C_4H_6O_4Ni \cdot 4H_2O$), polyvinylpyrrolidone (PVP k-30), hydrazine hydrate ($N_2H_4 \cdot H_2O$, 85%), glycerol, lactic acid, 1,2-propanediol, formic acid, acetic acid, oxalic acid, and isopropyl alcohol were of reagent grade and were purchased from Sinopharm chemical reagent Co., Ltd. All the chemicals were used as received without further purification. Deionized water was used through all the experiments.

2.2. Preparation of Hydroxyapatite

Nanosized hydroxyapatite (HAP) with rod-like shape was prepared according to the reported method.[40,41] Typically, equivalent volumes of calcium nitrate (1 mol L^{-1}) and phosphoric acid (0.6 mol L^{-1}) aqueous solutions were added into a three-necked round bottom flask. The aqueous solution was heated to 40 °C in a water bath. An ammonia solution (25%) was added dropwise into the solution to adjust its pH value of 10. After reacting at 40 °C for 4 h, the reaction solution was transferred into a Teflon-lined autoclave and autoclaved at 100 °C for 8 h. The resultant HAP sample was washed with distilled water until the conductivity of filtrate was less than 2 mS m^{-1}. Finally, the HAP sample was dried at 120 °C overnight. The as-prepared HAP nanorods were used as the catalyst support.

2.3. Preparation of Ni_x/HAP Catalyst

HAP-supported nickel catalysts (Ni_x/HAP; x, mole of Ni to the 100 g HAP) were prepared by the wetness chemical reduction method. A given amount of nickel acetate, PVP (PVP/Ni, m/m, 10:100), and 1 g of HAP powder were added in 60 mL of anhydrous ethanol by ultrasonic treatment for 30 min. The suspension was transferred into a three-necked round bottom flask and preheated to 60 °C in a thermostatic bath under stirring. A saturated NaOH anhydrous ethanol solution was added into the reaction mixture to adjust the pH value of 12. A hydrazine hydrate ethanol solution (8 mL in 100 mL anhydrous ethanol) was added dropwise to the reaction mixture and heated at 70 °C for 4 h under mild stirring. After reaction, the reaction mixture was cooled down to room temperature. The as-prepared Ni_x/HAP catalysts were filtrated and washed with anhydrous ethanol for three times and kept in an anhydrous ethanol solution before characterization and catalytic reaction. After filtration, the cake of the as-prepared Ni_x/HAP catalysts were directly used for catalytic reaction to prevent oxidation of metallic Ni^0 component. The Ni_x/HAP catalysts were donated as $Ni_{0.1}$/HAP, $Ni_{0.2}$/HAP, $Ni_{0.3}$/HAP, and $Ni_{0.4}$/HAP. The properties of the Ni_x/HAP catalysts are listed in Table I.

2.4. Characterization of HAP and Ni_x/HAP Catalysts

The X-ray powder diffraction (XRD) patterns of the metallic Ni^0, HAP, and Ni_x/HAP catalysts were recorded on a diffractometer (D8 super speed Bruker-AEX Company) using Cu Kα radiation ($\lambda = 1.54056$ Å) with Ni filter and scanning (2θ) from 10° to 80°. According to the Scherrer's equation: $D = K\lambda/(B\cos\theta)$, the crystallite sizes of Ni^0 nanoparticles (1 1 1) in the Ni_x/HAP catalysts were calculated. The value of K was taken as 1.0 and B was the full width of the diffraction line at half of the maximum of XRD peak of metallic Ni^0 (1 1 1). The results are listed in Table I.

The microstructures and the average particle sizes of the Ni_x/HAP catalysts were examined by transmission electron microscopy (TEM) and High-resolution transmission electron microscopy (HRTEM) on a microscope (JEM-2100) operated at an acceleration voltage of 200 kV. The sample was dispersed in anhydrous ethanol by ultrasonication for 10 min, then a drop of the ethanol suspension was placed onto a copper grid coated with a layer of amorphous carbon. The particle sizes of the Ni nanoparticles were estimated from the TEM and HRTEM images.

The basicities of the HAP and Ni_x/HAP catalysts were determined by the CO_2 temperature-programmed desorption (CO_2-TPD) technique in a fixed-bed continuous flow microreactor under atmospheric pressure. Firstly, the samples (0.1 g) were CO_2-saturated in a CO_2 stream at 60 °C for 0.5 h. After purging with helium stream with a flow rate of 30 mL min^{-1} at 60 °C for 0.5 h to remove the physically adsorbed CO_2, the samples were heated at 15 °C min^{-1} to 750 °C.

A NOVA 2000e physical adsorption apparatus was used to determine the specific surface areas of HAP and Ni_x/HAP catalysts by N_2 adsorption/desorption technique. The samples were degassed at 100 °C for 2 h under

Table I. Physicochemical properties of the catalysts.

Catalysts	Crystallite sizes of Ni^0 (1 1 1) (nm)[a]	Particle sizes of Ni^0 (nm)[b]	Specific surface areas (m^2/g)	Average pore diameters (nm)	Basic strength at different temperatures (μmol CO_2 g_{cat}^{-1})[c]	Total basicities (μmol CO_2 g_{cat}^{-1})
Ni	16.4	16	/	/	/	/
HAP	/	/	90.4	3.4	0.452 (117∼502 °C) 0.004 (585∼623 °C)	0.456
$Ni_{0.1}$/HAP	14.6	14	70.9	3.3	0.405 (137∼558 °C) 0.003 (559∼613 °C)	0.408
$Ni_{0.2}$/HAP	16.3	16	65.4	3.3	0.302 (140∼516 °C) 0.004 (555∼590 °C)	0.306
$Ni_{0.3}$/HAP	17.5	17	62.8	3.2	0.276 (171∼489 °C) 0.004 (533∼568 °C)	0.288
$Ni_{0.4}$/HAP	18.2	17	60.4	3.1	0.255 (179∼479 °C) 0.003 (522∼557 °C)	0.258

Notes: [a]Crystallite sizes of Ni^0 (nm) were calculated by Scherrer's equation. [b]The Particle sizes of Ni^0 (nm) were determined by TEM. [c]The total basicities of the Ni_x/HAP catalysts were calculated from CO_2-TPD curves.

vacuum before the measurement. The N_2 adsorption–desorption isotherms of the samples were measured at −196 °C. According to the BET method, the specific surface areas were calculated.

The compositions of the Ni_x/HAP catalysts and the concentrations of Ni^{2+} in reaction solutions were analyzed on an atomic absorption spectrophotometer (TAS-986). The results are listed in Table II.

2.5. Catalytic Test

Catalytic conversion of glycerol to lactic acid over Ni_x/HAP catalyst was carried out in a 300 mL stainless steel reactor with a mechanical stirrer. A given amount of Ni_x/HAP catalyst and 100 mL of aqueous solution of glycerol and NaOH were added into the reactor. Then the reactor was flushed with N_2 to replace air inside for 10 min before reaction. When the reaction temperature was raised to prescribed value, agitation started at 300 rpm. The reaction time was counted while the reaction temperature was raised to the prescribed value. After reacting for a certain time period, the reaction mixture was cooled down to room temperature for analysis.

Hydrochloric acid (37%) was used to adjust the pH of the reaction mixture to ca. 3 for HPLC analysis.[42]

Table II. The compositions of freshly and spent Ni_x/HAP catalysts and the concentration of Ni^{2+} in reaction solution.[a]

Catalysts	Mole of Ni to the 100 g HAP	Ni^{2+} (g L^{-1})
$Ni_{0.1}$/HAP	0.100:100	/
$Ni_{0.1}$/HAP (spent)	0.099:100	/
$Ni_{0.2}$/HAP	0.199:100	/
$Ni_{0.2}$/HAP (spent)	0.198:100	/
$Ni_{0.3}$/HAP	0.298:100	/
$Ni_{0.3}$/HAP (spent)	0.296:100	/
$Ni_{0.4}$/HAP	0.398:100	/
$Ni_{0.4}$/HAP (spent)	0.394:100	/
Reaction solution	/	Not detected

Note: [a]The experimental conditions: glycerol aqueous solution, 2 mol L^{-1}, 100 mL; Ni_x/HAP, 0.736 g; NaOH/glycerol mole ratio, 1.1:1; reaction temperature, 200 °C; reaction time, 2 h.

The organic acids present in the reaction mixture, such as lactic acid, acetic acid, oxalic acid, and formic acid, were analyzed on an Agilent HPLC system equipped with a tunable absorbance UV detector and a reverse-phase column (Innoval ASB C18, 5 μm, 100 Å, 4.6 mm × 250 mm) at 30 °C. The mobile phase was a methanol aqueous solution (10:90, V/V) with a flow rate of 0.8 mL min^{-1}. The pH value of the mobile phase was 2.3, which was adjusted with phosphate buffer. The detection wavelength was 210 nm. A gas-phase chromatograph (SP-6800A) equipped with a PEG-20 M packed capillary column (0.25 mm × 30 m) and a FID was used to analyze the concentrations of the unreacted glycerol and produced 1,2-propanediol. The isopropyl alcohol was used as the internal standard.

The product selectivity was calculated by carbon balance and the equation was listed as follows.

$$\text{Product selectivity} = (\text{Mole of product}) \times (\text{Carbon number of product molecule})/3(\text{Mole of consumed glycerol}) \quad (1)$$

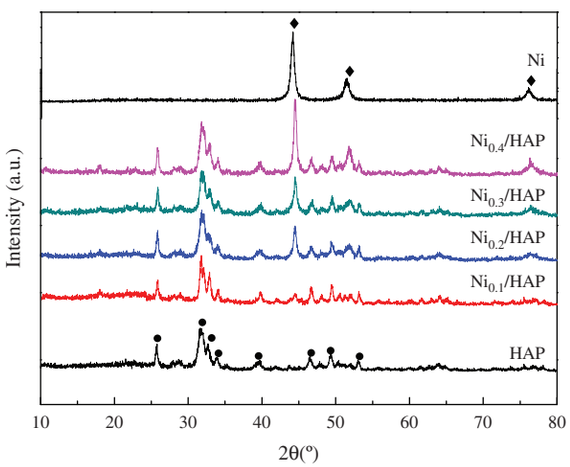

Figure 1. XRD patterns of the hydroxyapatite, metallic Ni^0, and fresh Ni_x/HAP catalysts. ●, HAP; ♦, Ni^0.

3. RESULTS AND DISCUSSION

3.1. XRD and AAS Analyses

The XRD patterns of metallic Ni^0, HAP, and Ni_x/HAP catalysts are shown in Figure 1. The XRD peaks of the metallic Ni^0 and Ni_x/HAP catalysts appearing at $2\theta = 44.5$, 51.9, and 76.4° were indexed as the (1 1 1), (2 0 0), and (2 2 0) planes of face centered-cubic (fcc) nickel (JCPDS 04-0850), respectively. No nickel oxides and nickel hydroxides were detected, indicating that metallic Ni^0 nanoparticles were prepared under the present experimental conditions. The peak intensities of metallic Ni^0 in the Ni_x/HAP catalysts increased with the increase in nickel loadings. The crystallite sizes of Ni^0 in the Ni_x/HAP catalysts in a range of 14.6–18.2 nm were estimated by Scherrer's equation, indicating that the metallic Ni^0 particles in Ni_x/HAP catalysts were nanometer magnitude (Table I). The crystallite sizes of the metallic Ni^0 in the Ni_x/HAP catalysts increased with the increase in nickel loadings.

The XRD peaks of the HAP and Ni_x/HAP catalysts appearing at $2\theta = 25.9$, 31.8, 32.2, 32.9, 34.1, 39.8, 46.7, 49.5, and 53.1° were ascribed to those of standard hydroxyapatite (JCPDS 09-0432). The supports in the catalysts were still in hydroxyapatite phase.

The nickel contents in the fresh and spent Ni_x/HAP catalysts analyzed by AAS are shown in Table II. The nickel contents in the fresh catalysts were close to those in the spent ones, correspondingly. There was no nickel detected

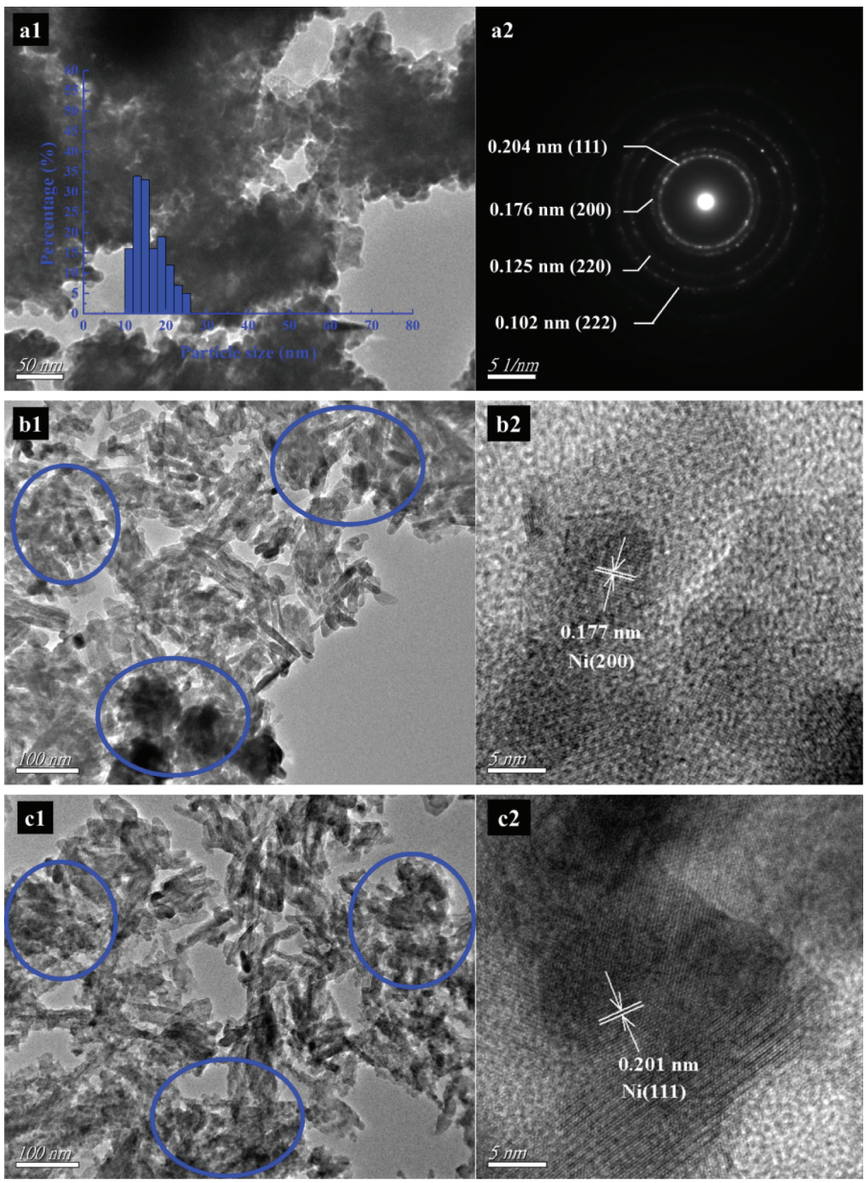

Figure 2. Continued.

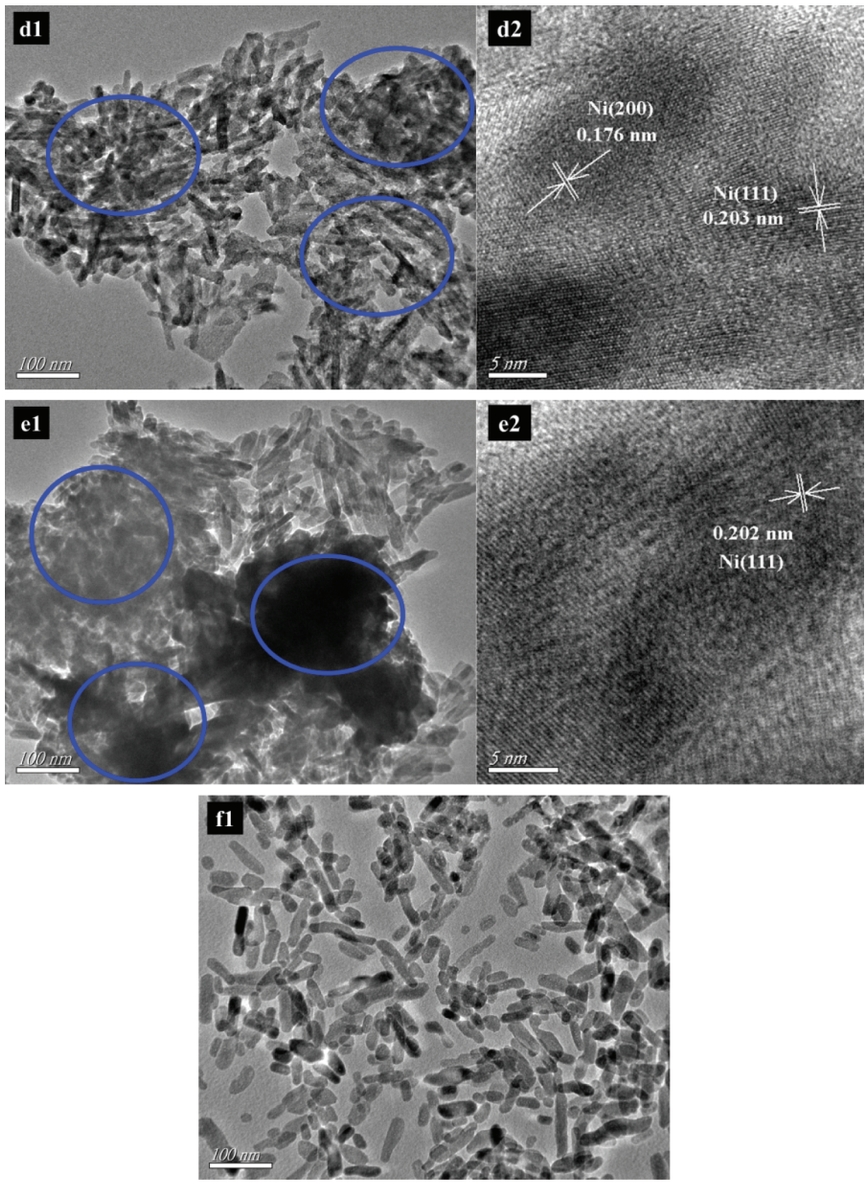

Figure 2. TEM, SAED, HRTEM images of (a1, a2) metallic Ni^0, (b1, b2) $Ni_{0.1}$/HAP, (c1, c2) $Ni_{0.2}$/HAP, (d1, d2) $Ni_{0.3}$/HAP, (e1, e2) $Ni_{0.4}$/HAP, and (f1) HAP support. The typical supported Ni^0 nanoparticles are marked by circling in the TEM images.

in the reaction solution. The results revealed that the metallic Ni^0 nanoparticles could attach at the HAP surfaces tightly.

3.2. TEM and HRTEM Analyses

The TEM, SAED, and HRTEM images of the metallic Ni^0, HAP support, and Ni_x/HAP catalysts are shown in Figure 2. The TEM image shows that the metallic Ni^0 sample was composed of spherical nanoparticles with the average particle size of 16 nm and the particle size distribution of 10–25 nm (Table I). According to the SAED pattern (Fig. 2(a2)), the diffraction fringes of the metallic Ni^0 sample were close to the {1 1 1} (0.204 nm), {2 0 0} (0.176 nm), {2 2 0} (0.125 nm), and {2 2 2} (0.102 nm) lattice spacings of fcc nickel, respectively. The metallic Ni^0 nanoparticles had a poly-crystalline structure.

The TEM image shows that the HAP support was nanorod with the average diameter and length of ca. 16 and 58 nm, respectively (Fig. 2(f1)). The TEM images of the Ni_x/HAP catalysts show that the supported Ni^0 nanoparticles had the average particle sizes in a range of 14–17 nm (Figs. 2(b1–e1)). The lattice fringes of the Ni^0 nanoparticles in the Ni_x/HAP catalysts were around 0.203 and 0.176 nm, being close to the {1 1 1} and {2 0 0} lattice spacings of fcc metallic nickel (Figs. 2(b2–e2)).

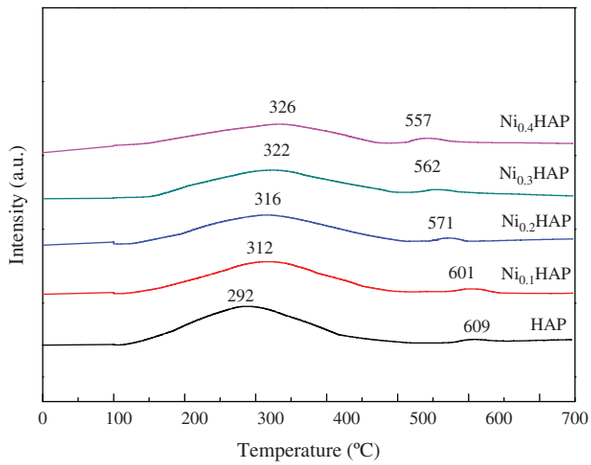

Figure 3. CO_2-TPD patterns of HAP support and Ni_x/HAP catalysts.

Table III. Catalytic conversion of glycerol with the use of sole NaOH or $Ni_{0.2}$/HAP catalyst.

Catalysts	Reaction time (h)	Conversions of glycerol (%)	Selectivities of lactic acid (%)
NaOH[a]	1	Trace	/
	2	Trace	/
	3	Trace	/
	4	0.9	100
$Ni_{0.2}$/HAP[b]	1	Trace	/
	2	Trace	100
	3	1.8	100
	4	2.9	99.8

Notes: [a]Glycerol aqueous solution, 2.0 mol L^{-1}, 100 mL; NaOH/glycerol mole ratio, 1.1:1; reaction temperature, 200 °C. [b]Glycerol aqueous solution, 2.0 mol L^{-1}, 100 mL; $Ni_{0.2}$/HAP, 0.736 g; reaction temperature, 200 °C.

3.3. CO_2-TPD Analysis

To investigate the surface basicities of the HAP support and Ni_x/HAP catalysts, the CO_2-TPD was carried out (Fig. 3). Their basic strengths are listed in Table I.

The HAP support and $Ni_{0.1}$/HAP, $Ni_{0.2}$/HAP, $Ni_{0.3}$/HAP, $Ni_{0.4}$/HAP catalysts exhibited two CO_2 desorption peaks at 292, 609; 312, 601; 316, 571; 322, 562; 326, 557 °C, respectively. Generally, the CO_2 desorption peaks in the regions of 100–250, 250–450, and 450–700 °C are assigned to CO_2 desorption from weak-, medium-, and strong-strength basic sites, respectively.[43, 44] Therefore, the HAP support and Ni_x/HAP catalysts possessed both medium- and strong-strength basic sites. Their medium-strength basicities were obviously higher than their strong-strength basicities. However, the total basicities of the Ni_x/HAP catalysts decreased with the increase in the Ni contents, revealing that metallic Ni^0 nanoparticles covered the support surface, resulting in a decrease in the basicity.

3.4. BET Analysis

The specific surface areas and average pore sizes of the HAP support and Ni_x/HAP catalysts are listed in Table I. The specific surface areas of the HAP support and Ni_x/HAP catalysts decreased from 90.4 to 60.4 m^2 g^{-1} with increasing the Ni loadings. The average pore diameters slightly decreased from 3.4 to 3.1 nm. The decrease in the specific surface area and average pore diameter with the increase in Ni loadings was probably due to that the pores of HAP support were partially choked by supported metallic Ni^0 nanoparticles.

3.5. Catalytic Conversion of Glycerol to Lactic Acid

3.5.1. Catalytic Activities of Ni_x/HAP Catalysts

Before investigating the catalytic activities of Ni_x/HAP catalysts, the sole $Ni_{0.2}$/HAP catalyst or NaOH was used in the catalytic conversion of glycerol (2.0 mol L^{-1}), after reacting at 200 °C for 4 h, the glycerol conversions were less than 3% and lactic acid was the main product (Table III). When both Ni_x/HAP catalyst and NaOH were used in the catalytic conversion of glycerol, the glycerol conversions and the lactic acid selectivities were above 79.0% and 89.5%, respectively (Table IV). It was reasonable to conclude that NaOH and supported Ni_x/HAP catalysts synergistically catalyzed the conversion of glycerol to lactic acid.

When the Ni_x/HAP catalysts were used for catalyzing the hydrothermal conversion of glycerol (2.0 mol L^{-1}) in a NaOH (2.2 mol L^{-1}) aqueous solution, after reacting at 200 °C for 2 h, the glycerol conversions increased

Table IV. The effect of Ni content in the catalysts on catalytic conversion of glycerol to lactic acid.

		Selectivities (%)							
Catalysts	Conversions[a] (%)	Lactic acid	Oxalic acid	Formic acid	Acetic acid	1,2-Propanediol	Activities for glycerol conversion[b] (h^{-1})	Activities for lactic acid formation[c] (h^{-1})	Carbon balances[d] (%)
Ni	73.9	89.5	0.3	4.9	2.0	1.0	47.2	42.2	97.7
HAP	1.7	65.3	5.6	6.6	21.9	0	0	0	99.4
$Ni_{0.1}$/HAP	79.2	93.7	0.4	1.2	0.4	1.0	113.9	106.7	96.7
$Ni_{0.2}$/HAP	92.1	94.7	0.4	1.8	0.5	1.0	69.9	66.2	98.4
$Ni_{0.3}$/HAP	94.0	92.3	0.6	2.0	0.6	1.2	50.1	46.2	96.7
$Ni_{0.4}$/HAP	96.0	89.8	0.8	2.2	0.8	1.5	40.3	36.2	95.1

Notes: [a]Reaction conditions: glycerol aqueous solution, 100 mL, 2.0 mol L^{-1}; NaOH/glycerol molar ratio 1.1:1; metallic Ni catalyst, 0.92 g; Ni_x/HAP catalyst, 0.736 g; reaction temperature 200 °C; reaction time, 2.0 h. [b]Glycerol conversion activities normalized per metal atom. [c]Lactic acid formation activities normalized per metal atom. [d]Carbon balances were calculated according to both detected products and reacted glycerol.

from 79.2% to 96.0% with the increase in metallic Ni^0 loadings (Table IV). The selectivities of lactic acid were in a range of 89.8%–94.7%. The selectivities of by-products (oxalic acid, formic acid, acetic acid, and 1,2-propanediol) were less than 2.2%, respectively. The Ni_x/HAP catalysts exhibited high catalytic activities for the catalytic conversion of glycerol to lactic acid. The $Ni_{0.2}$/HAP catalyst gave the highest lactic acid yield of 87.2%, indicating that the Ni content also affected the product yield.

The carbon balance values over the Ni_x/HAP catalysts were above 95.0%. The results revealed that the Ni_x/HAP catalysts effectively catalyzed the hydrothermal conversion of glycerol to the detected chemicals.

The catalytic activities of the $Ni_{0.1}$/HAP and $Ni_{0.2}$/HAP catalysts for glycerol conversion were 1.5 and 2.4 times that of the sole metallic Ni^0 nanoparticle catalyst, respectively (Table IV). The catalytic activities of the $Ni_{0.1}$/HAP and $Ni_{0.2}$/HAP catalysts for lactic acid formation were 1.6 and 2.5 times that of the sole metallic Ni^0 nanoparticle

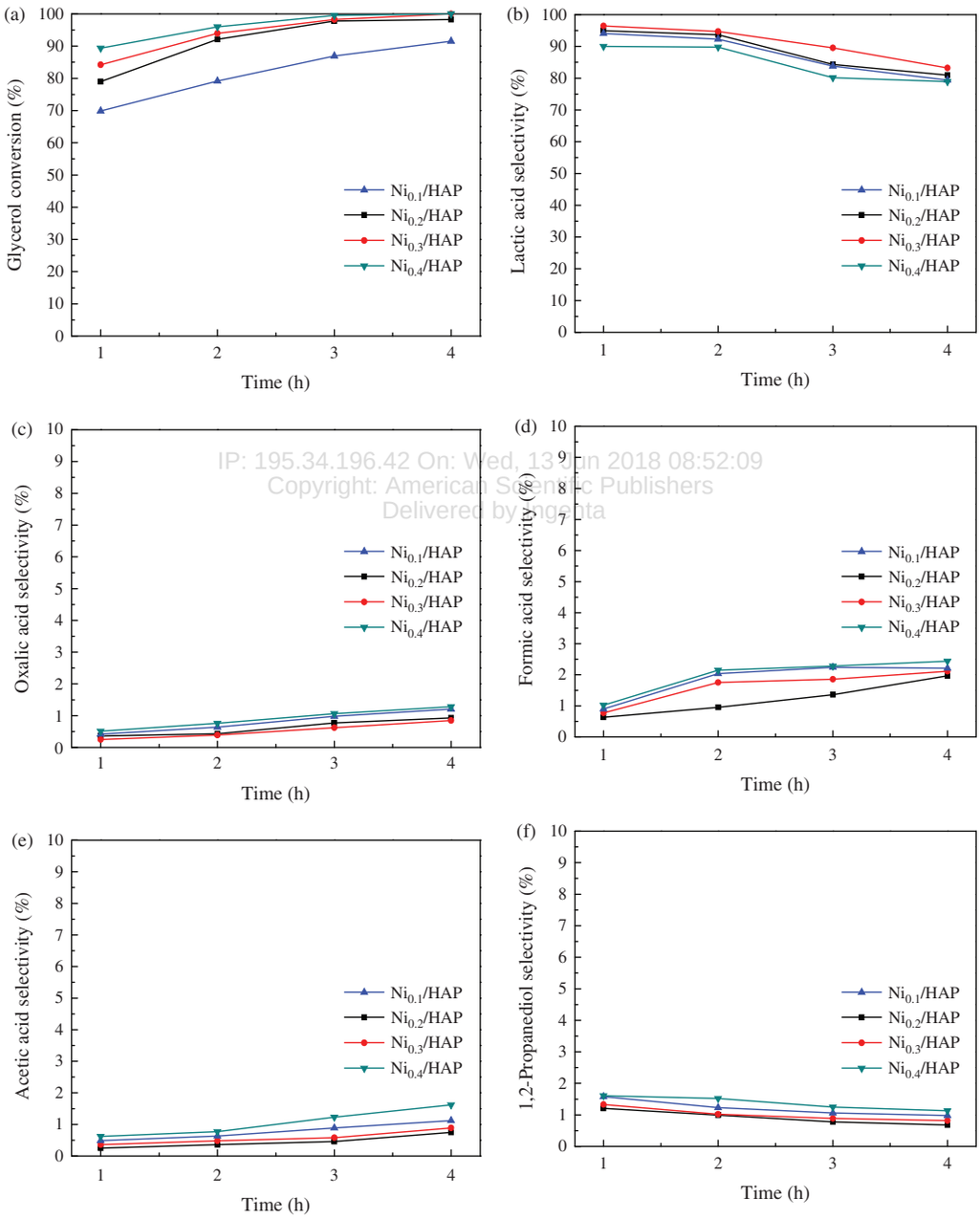

Figure 4. Catalytic conversion of glycerol catalyzed by the Ni_x/HAP catalysts. Reaction conditions: glycerol aqueous solution, 100 mL, 2 mol L^{-1}; NaOH/glycerol mole ratio, 1.1:1; catalyst, 0.736 g; and reaction temperature, 200 °C.

catalyst. The catalytic activities of the $Ni_{0.3}$/HAP and $Ni_{0.4}$/HAP catalysts for glycerol conversion and lactic acid formation were comparable to those of the sole metallic Ni^0 nanoparticle catalyst. The content of the Ni^0 nanoparticles in the Ni_x/HAP catalysts obviously affected the conversion of glycerol to lactic acid.

3.5.2. Effect of Reaction Time

When the catalytic conversion of glycerol (2.0 mol L^{-1}) was catalyzed by the $Ni_{0.1}$/HAP, $Ni_{0.2}$/HAP, $Ni_{0.3}$/HAP, and $Ni_{0.4}$/HAP catalysts at 200 °C, with prolonging the reaction time to 4.0 h, the conversions of glycerol increased to 91.5%, 98.3%, 100%, and 100%, respectively (Fig. 4(a)). After reacting for 1 h, the maximum lactic acid selectivities of 95.0%, 96.4%, 94.1%, and 90.0% were obtained, respectively. With prolonging the reaction time to 4.0 h, the selectivities of lactic acid decreased to 81.0%, 83.2%, 79.4%, and 79.0%. The selectivities of the by-products were less than 2.9%, respectively (Figs. 4(c–f)).

Over the Ni_x/HAP catalysts, the maximum yields of lactic acid were obtained at 2 h. The reaction time period of 2 h was fixed to investigate the effect of other reaction parameters on the catalytic conversion of glycerol.

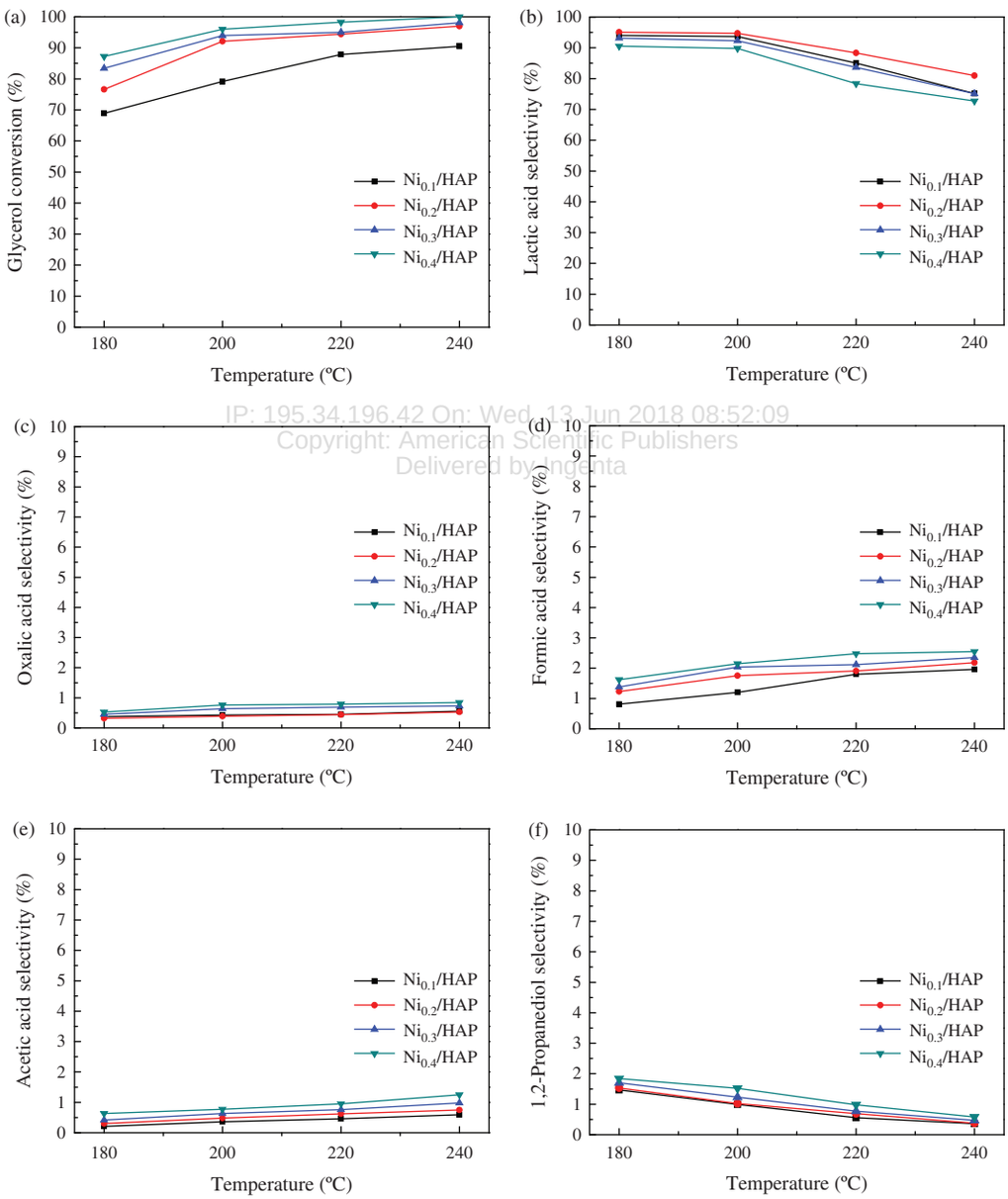

Figure 5. Catalytic conversion of glycerol catalyzed by the Ni_x/HAP catalysts. Reaction conditions: glycerol aqueous solution, 100 mL, 2 mol L^{-1}; NaOH/glycerol mole ratio, 1.1:1; catalyst, 0.736 g; and reaction time, 2 h.

3.5.3. Effect of Reaction Temperature

The glycerol conversions and product selectivities in the catalytic conversion of glycerol over the $Ni_{0.1}$/HAP, $Ni_{0.2}$/HAP, $Ni_{0.3}$/HAP, and $Ni_{0.4}$/HAP catalysts at different reaction temperatures are shown in Figure 5. With increasing the reaction temperature from 180 °C to 240 °C, the glycerol conversions increased to 90.5%, 97.0%, 98.1%, and 100%, respectively. The selectivities of lactic acid decreased from 94.0% to 75.2%, 95.1% to 81.0%, 93.1% to 75.1%, and 90.5% to 72.7%, respectively. When the reaction temperature was 200 °C, the maximum lactic acid yields of 74.2%, 87.2%, 86.7%, and 86.2% were obtained, respectively. The selectivities of the by-products were all less than 2.6%. The optimal reaction temperature was 200 °C from the perspective of lactic acid yield.

3.5.4. Effect of Glycerol Concentration

The glycerol conversion and lactic acid selectivity over the Ni_x/HAP catalysts decreased upon increasing glycerol concentration (Table V). The $Ni_{0.2}$/HAP and $Ni_{0.3}$/HAP catalysts exhibited high catalytic activities for the conversion of high-concentrated glycerol (1.5–3.0 mol L^{-1}) to lactic acid with the lactic acid selectivities of 82.6%–95.6% at the glycerol conversions of 92.1%–97.7%. When the glycerol concentration was 1.5 mol L^{-1}, the maximum lactic acid yields over the $Ni_{0.2}$/HAP and $Ni_{0.3}$/HAP catalysts were 92.8% and 91.5%, respectively. The selectivities of the by-products were less than 2.3%, respectively. The carbon balances over the Ni_x/HAP catalysts decreased from ca. 99% to 85% upon increasing the glycerol concentrations from 1.5 to 3.0 mol L^{-1}, meaning that high glycerol concentration probably caused the formation of undetected products.

The catalytic activities for glycerol conversion and lactic acid formation based on metallic Ni^0 increased upon increasing glycerol concentration, indicating that metallic Ni^0 sites could effectively catalyze the glycerol conversion to lactic acid.

3.5.5. Effect of NaOH/Glycerol Mole Ratio

With increasing the NaOH/glycerol mole ratios from 1.0:1 to 1.3:1, the conversions of glycerol over the $Ni_{0.1}$/HAP, $Ni_{0.2}$/HAP, $Ni_{0.3}$/HAP, and $Ni_{0.4}$/HAP catalysts increased to 84.4%, 95.9%, 97.5%, and 98.0%, respectively (Fig. 6). The selectivities of lactic acid decreased from 94.8% to 86.8%, 95.6% to 89.1%, 93.6% to 82.8%, and 91.3% to 80.8%. The selectivities of the by-products were less than 2.9%. High NaOH/glycerol mole ratio favored the catalytic conversion of glycerol. But excessive NaOH content decreased the selectivity of lactic acid.

3.5.6. Effect of Catalyst Loading

With increasing the catalyst loadings from 0.368 to 0.920 g, the conversions of glycerol over the $Ni_{0.1}$/HAP, $Ni_{0.2}$/HAP, $Ni_{0.3}$/HAP, and $Ni_{0.4}$/HAP catalysts increased to 86.2%, 96.3%, 98.8%, and 99.5%, respectively (Table VI). The selectivities of lactic acid decreased from ca. 95% to 81%. The selectivities of the by-products were less than 2.3%, respectively. The results revealed that high catalyst loading gave a high glycerol conversion while the excessive catalyst loading caused the decrease in lactic acid selectivity. To obtain high lactic acid yield, the optimal catalyst loading was around 0.7 g.

Table V. Effect of glycerol concentration on catalytic conversion of glycerol to lactic acid.[a]

Catalysts	Glycerol concentrations (mol L^{-1})	Glycerol conversions (%)	Selectivities (%)					Activities for glycerol conversion[b] (h^{-1})	Activities for lactic acid formation[c] (h^{-1})	Carbon balances[d] (%)
			Lactic acid	Oxalic acid	Formic acid	Acetic acid	1,2-Propanediol			
$Ni_{0.1}$/HAP	1.5	83.8	94.7	0.2	1.6	0.3	1.5	90.4	85.7	98.3
	2.0	79.2	93.7	0.4	1.0	0.4	1.0	113.9	106.7	96.5
	2.5	74.7	86.4	0.5	0.8	0.8	0.6	134.3	116.1	89.1
	3.0	68.4	83.6	0.5	0.7	0.9	0.5	147.5	123.3	86.2
$Ni_{0.2}$/HAP	1.5	97.1	95.6	0.2	1.9	0.4	1.6	55.3	52.8	99.7
	2.0	92.1	94.7	0.4	1.8	0.5	1.0	69.9	66.2	98.4
	2.5	95.0	87.8	0.5	1.2	0.9	0.7	90.1	79.1	91.1
	3.0	94.1	85.0	0.5	0.9	0.9	0.7	107.2	91.1	88.0
$Ni_{0.3}$/HAP	1.5	97.7	93.7	0.2	2.2	0.6	1.8	39.0	36.6	98.5
	2.0	94.0	92.3	0.6	2.0	0.6	1.2	50.1	46.2	96.7
	2.5	95.3	85.4	0.7	1.3	1.0	1.0	63.4	54.2	89.4
	3.0	94.6	82.6	0.8	1.1	1.2	1.0	75.6	62.5	86.7
$Ni_{0.4}$/HAP	1.5	98.6	91.1	0.3	2.3	0.7	1.9	31.0	28.3	96.3
	2.0	96.0	89.8	0.8	2.2	0.8	1.5	40.3	36.2	95.1
	2.5	88.8	84.5	0.8	1.5	1.3	1.2	46.5	39.3	89.3
	3.0	80.9	80.6	0.9	1.2	1.4	1.0	50.9	41.0	85.1

Notes: [a]Reaction conditions: glycerol aqueous solution, 100 mL; NaOH/glycerol mole ratio, 1.1:1; catalyst loading, 0.736 g; reaction temperature, 200 °C; reaction time, 2.0 h. [b]Glycerol conversion activities normalized per metal atom. [c]Lactic acid formation activities normalized per metal atom. [d]Carbon balances were calculated according to both detected products and reacted glycerol.

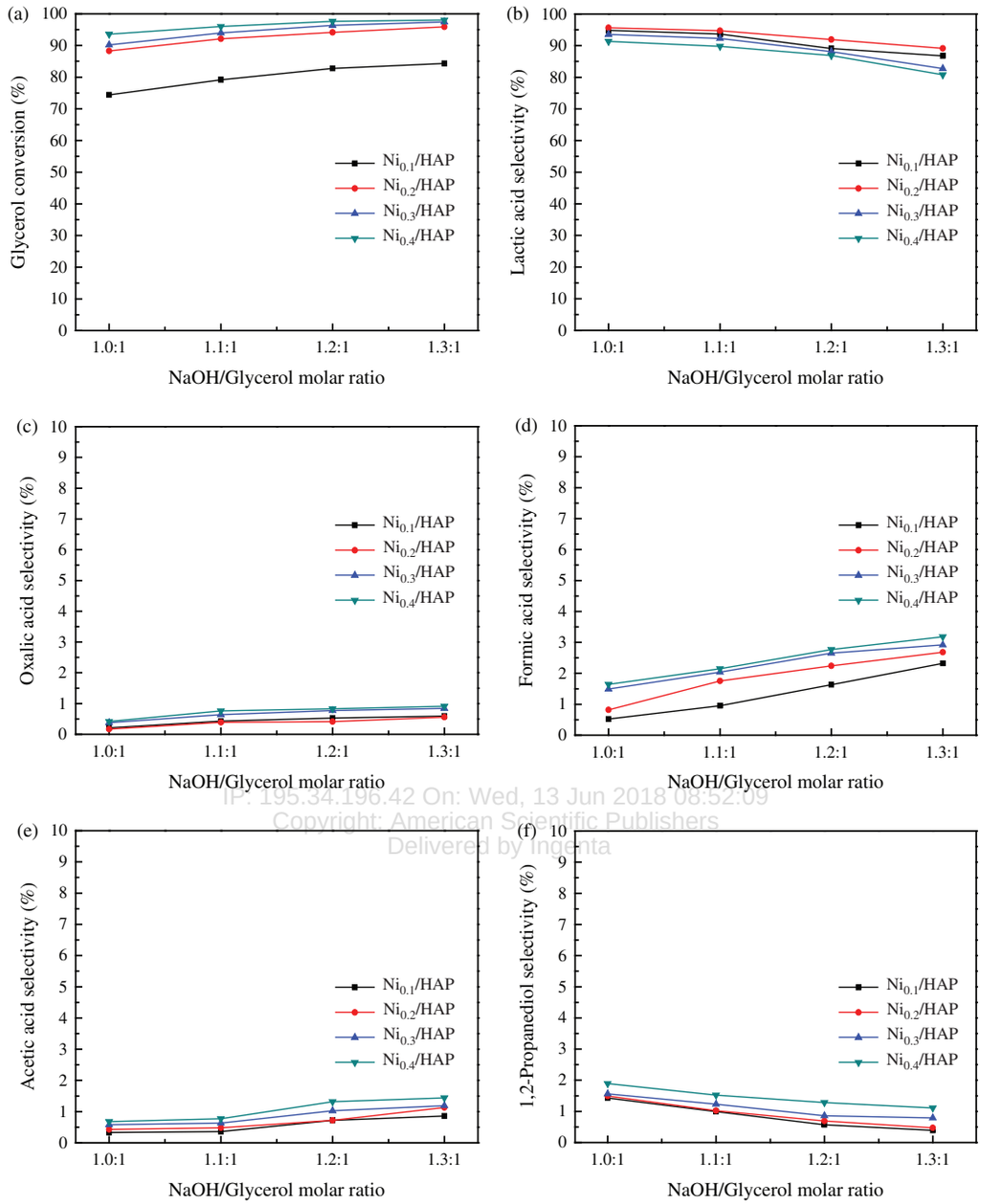

Figure 6. Catalytic conversion of glycerol catalyzed by the Ni_x/HAP catalysts. Reaction conditions: glycerol aqueous solution, 100 mL, 2 mol L^{-1}; catalyst, 0.736 g; reaction temperature, 200 °C; reaction time, 2 h.

3.6. Possible Reaction Routes

According to the findings in our present work and the reported reaction pathways for the catalytic conversion of glycerol to lactic acid in an aqueous solution,[23, 26, 45, 46] the possible reaction routes over the Ni_x/HAP catalysts in an alkaline solution are summarized as follows (Scheme 1).

The supported metallic nickel nanoparticles catalyzed the dehydrogenation of terminal hydroxyl group of glycerol to glyceraldehyde. 2-Hydroxypropenal was formed from the intramolecular dehydration of glyceraldehyde in a basic environment.[33, 45] Pyruvaldehyde was formed from 2-hydroxypropenal via the keto-enol tautomerization.[46] The resultant pyruvaldehyde was converted to lactate via the Cannizaro reaction.[23, 29, 30, 33]

For the byproducts, 1,2-propanediol was formed by the hydrogenation of glycerol with resultant H_2 over the Ni_x/HAP catalysts.[47, 48] The acetate and formate anions were formed by the decomposition of lactate anions in an alkaline solution, respectively.[33] The oxalate anions were probably formed by the cleavage of glyceraldehyde.[33, 34]

Table VI. Effect of catalyst loading on catalytic conversion of glycerol to lactic acid.[a]

Catalysts	Catalyst loadings (g)	Glycerol conversions (%)	Selectivities (%)					Activities for glycerol conversion[b] (h^{-1})	Activities for lactic acid conversion[c] (h^{-1})	Carbon balances[d] (%)
			Lactic acid	Oxalic acid	Formic acid	Acetic acid	1,2-Propanediol			
$Ni_{0.1}$/HAP	0.368	63.4	94.9	0.1	0.5	1.1	1.7	182.3	173.0	98.3
	0.552	72.7	94.6	0.3	0.6	0.9	1.2	139.5	132.0	97.6
	0.736	79.2	93.7	0.4	1.0	0.4	1.0	113.9	106.7	96.5
	0.920	86.2	82.7	0.5	1.4	0.4	0.6	99.2	82.1	85.6
$Ni_{0.2}$/HAP	0.368	76.8	95.9	0.1	0.6	1.3	1.5	116.6	111.9	99.4
	0.552	84.2	95.8	0.2	1.0	1.0	1.4	85.2	81.6	99.4
	0.736	92.1	94.7	0.4	1.8	0.5	1.0	69.9	66.2	98.4
	0.920	96.3	83.6	0.5	1.9	0.4	0.8	58.5	48.9	87.2
$Ni_{0.3}$/HAP	0.368	80.6	94.5	0.2	1.0	1.3	1.8	85.9	81.1	98.8
	0.552	88.0	93.9	0.4	1.4	1.1	1.4	62.5	58.7	98.2
	0.736	94.0	92.3	0.6	2.0	0.6	1.2	50.1	46.2	96.7
	0.920	98.8	81.2	0.7	2.1	0.5	1.0	42.1	34.2	85.5
$Ni_{0.4}$/HAP	0.368	87.0	93.6	0.2	1.3	1.6	2.1	73.0	68.3	98.8
	0.552	91.8	91.6	0.4	1.7	1.2	1.8	51.3	47.0	96.7
	0.736	96.0	89.8	0.8	2.2	0.8	1.5	40.3	36.2	95.1
	0.920	99.5	80.2	0.9	2.3	0.7	1.3	33.4	26.8	85.4

Notes: [a]Reaction conditions: glycerol aqueous solution, 2.0 mol L^{-1}, 100 mL; NaOH/glycerol mole ratio, 1.1:1; reaction temperature, 200 °C; reaction time, 2.0 h. [b]Glycerol conversion activities normalized per metal atom. [c]Lactic acid formation activities normalized per metal atom. [d]Carbon balances were calculated according to both detected products and reacted glycerol.

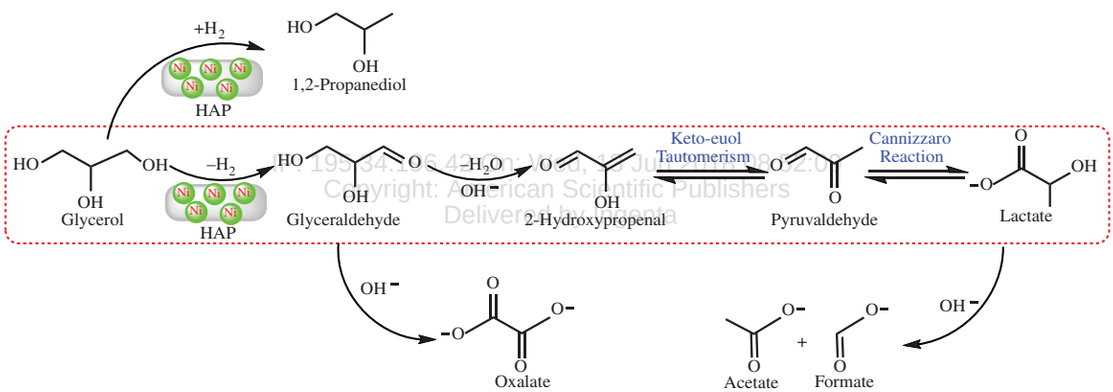

Scheme 1. Reaction routes for catalytic conversion of high-concentrated glycerol to lactic acid over the Ni_x/HAP catalysts in a NaOH aqueous solution.

In our present work, some intermediates, such as pyruvaldehyde, glyceraldehyde, and 2-hydroxypropenal were not detected under our present experimental conditions, indicating that these intermediates could be rapidly converted to subsequent chemicals and finally to lactate and by-products.

4. CONCLUSIONS

The HAP-supported metallic Ni^0 nanoparticles were prepared by the wet chemical reduction method. The average particle sizes of metallic Ni^0 nanoparticles on the surfaces of HAP ranged from 14 to 17 nm. For the catalytic reaction, metallic Ni^0 nanoparticles and NaOH synergistically catalyzed glycerol conversion to lactic acid. The $Ni_{0.2}$/HAP and $Ni_{0.3}$/HAP catalysts exhibited high catalytic activities for the conversion of high-concentrated glycerol (1.5–3.0 mol L^{-1}) to lactic acid with the lactic acid selectivities of 82.6%–95.6% at the glycerol conversions of 92.1%–97.7%. The Ni_x/HAP effectively catalyzed the conversion of high-concentrated glycerol to lactic acid at a relatively lower reaction temperature as compared to the hydrothermal conversion of glycerol to lactic acid in a NaOH aqueous solution.

Acknowledgments: The work was financially supported by the funds from National Natural Science Foundation of China (21506078 and 21506082) and China Postdoctoral Science Foundation (2016M601739).

References and Notes

1. Y. Hirano, Y. Kasai, K. Sagata, and Y. Kita, *Bull. Chem. Soc. Jpn.* 89, 1026 **(2016)**.
2. M. Dusselier, R. De Clercq, R. Cornelis, and B. F. Sels, *Catal. Today* 279, 339 **(2017)**.

3. B. Chen, F. Li, Z. Huang, and G. Yuan, *Appl. Catal. B* 200, 192 (**2017**).
4. L. Chen, S. Ren, and X. P. Ye, *Reac. Kinet. Mech. Cat.* 114, 93 (**2015**).
5. D. T. Johnson and K. A. Taconi, *Environ. Prog.* 26, 338 (**2007**).
6. A. B. F. Moreira, A. M. Bruno, M. M. V. M. Souza, and R. L. Manfro, *Fuel Process. Technol.* 144, 170 (**2016**).
7. A. Abuadala and I. Dincer, *Int. J. Energy Res.* 36, 415 (**2012**).
8. N. S. Bentsen and C. Felby, *Biotechnol. Biofuels* 5, 25 (**2012**).
9. A. V. Bridgwater, *Chem. Eng. J.* 91, 87 (**2003**).
10. L. Faba, E. Díaz, and S. Ordóñezn, *Renew. Sust. Energ. Rev.* 51, 273 (**2015**).
11. S. E. Hosseini, M. A. Wahid, M. M. Jamil, A. A. M. Azli, and M. F. Misbah, *Int. J. Energ. Res.* 39, 1597 (**2015**).
12. G. W. Huber, S. Iborra, and A. Corma, *Chem. Rev.* 106, 4044 (**2006**).
13. E. D. Revellame, W. E. Holmes, T. J. Benson, A. L. Forks, W. T. French, and R. Hernandez, *Top Catal.* 55, 185 (**2012**).
14. M. R. A. Arcanjo, I. J. Silva Jr., E. Rodríguez-Castellón, A. Infantes-Molina, and R. S. Vieira, *Catal. Today* 279, 317 (**2017**).
15. S. Adhikari, S. D. Fernando, and A. Haryanto, *Renew. Energ.* 33, 1097 (**2008**).
16. R. Moita, A. Freches, and P. C. Lemos, *Water Res.* 58, 9 (**2014**).
17. R. K. Saxena, P. Anand, S. Saran, and J. Isar, *Biotechnol. Adv.* 27, 895 (**2009**).
18. Z. Shen, F. Jin, Y. Zhang, B. Wu, A. Kishita, K. Tohji, and H. Kishida, *Ind. Eng. Chem. Res.* 48, 8920 (**2009**).
19. C. Zhang, T. Wang, X. Liu, and Y. Ding, *Chinese J. Catal.* 37, 502 (**2016**).
20. Z. Lu, I. Demianets, R. Hamze, N. J. Terrile, and T. J. Williams, *ACS Catal.* 6, 2014 (**2016**).
21. R. E. Drumright, P. R. Gruber, and D. E. Henton, *Adv. Mater.* 12, 1841 (**2000**).
22. G. Dreschke, M. Probst, A. Walter, T. Pümpel, J. Walde, and H. Insam, *Bioresource Technol.* 176, 47 (**2015**).
23. C. A. Ramírez-López, J. R. Ochoa-Gómez, M. Fernández-Santos, O. Gómez-Jiménez-Aberasturi, A. Alonso-Vicario, and J. Torrecilla-Soria, *Ind. Eng. Chem. Res.* 49, 6270 (**2010**).
24. W. He, G. Li, L. Kong, H. Wang, J. Huang, and J. Xu, *Resour. Conserv. Recy.* 52, 691 (**2008**).
25. H. Oh, Y. J. Wee, J. S. Yun, and H. W. Ryu, *Appl. Biochem. Biotechnol.* 105–108, 603 (**2003**).
26. H. Kishida, F. Jin, Z. Zhou, T. Moriya, and H. Enomoto, *Chem. Lett.* 34, 11 (**2005**).
27. T. Shimanouchi, S. Ueno, K. Shidahara, and Y. Kimura, *Chem. Lett.* 43, 535 (**2014**).
28. Y. Shen, S. Zhang, H. Li, Y. Ren, and H. Liu, *Chem. Eur. J.* 16, 7368 (**2010**).
29. P. Lakshmanan, P. P. Upare, N. Le, Y. K. Hwang, D. W. Hwang, U. Lee, H. R. Kim, and J. Chang, *Appl. Catal. A-Gen.* 468, 260 (**2013**).
30. R. K. P. Purushothaman, J. V. Haveren, D. S. V. Es, I. Melián-Cabrera, J. D. Meeldijk, and H. J. Heeres, *Appl. Catal. B-Environ.* 147, 92 (**2014**).
31. J. Ftouni, N. Villandier, F. Auneau, M. Besson, L. Djakovitch, and C. Pinel, *Catal. Today* 257, 267 (**2015**).
32. D. Roy, B. Subramaniam, and R. V. Chaudhari, *ACS Catal.* 1, 548 (**2011**).
33. H. X. Yin, C. Zhang, H. B. Yin, D. Gao, L. Shen, and A. Wang, *Chem. Eng. J.* 288, 332 (**2016**).
34. H. Yin, H. B. Yin, A. Wang, L. Shen, Y. Liu, and Y. Zheng, *J. Nanosci. Nanotechnol.* 17, 1255 (**2016**).
35. Y. Feng, H. Yin, A. Wang, T. Xie, and T. Jiang, *Appl. Catal. A* 425–426, 205 (**2012**).
36. Y. Du, H. Chen, R. Chen, and N. Xu, *Appl. Catal. A-Gen.* 277, 259 (**2004**).
37. A. L. Wang, H. B. Yin, M. Ren, H. H. Lu, J. J. Xue, and T. S. Jiang, *New J. Chem.* 34, 708 (**2010**).
38. A. Wang, H. Yin, H. Lu, J. Xue, M. Ren, and T. Jiang, *Catal. Commun.* 10, 2060 (**2009**).
39. A. Wang, H. Yin, H. Lu, J. Xue, M. Ren, and T. Jiang, *Langmuir* 25, 12736 (**2009**).
40. A. Wang, H. Yin, D. Liu, H. Wu, Y. Wada, M. Ren, Y. Xu, T. Jiang, and X. Cheng, *Appl. Surf. Sci.* 253, 3311 (**2007**).
41. A. Wang, D. Liu, H. Yin, H. Wu, Y. Wada, M. Ren, T. Jiang, X. Cheng, and Y. Xu, *Mater. Sci. Eng. C* 27, 865 (**2007**).
42. Y. Feng, H. Yin, D. Gao, A. Wang, L. Shen, and M. Meng, *J. Catal.* 316, 67 (**2014**).
43. E. Santacesaria, G. Carotenuto, R. Tesser, and M. Di Serio, *Chem. Eng. J.* 179, 209 (**2012**).
44. D. Gao, Y. Feng, H. Yin, A. Wang, and T. Jiang, *Chem. Eng. J.* 233, 349 (**2013**).
45. L. Chen, S. Ren, and X. P. Ye, *Fuel Process. Technol.* 120, 40 (**2014**).
46. F. Auneau, C. Michel, F. Delbecq, C. Pinel, and P. Sautet, *Chem. Eur. J.* 17, 14288 (**2011**).
47. G. Y. Yang, Y. H. Ke, H. F. Ren, C. L. Liu, R. Z. Yang, and W. S. Dong, *Chem. Eng. J.* 283, 759 (**2016**).
48. Y. Feng, H. Yin, L. Shen, A. Wang, Y. Shen, and T. Jiang, *Chem. Eng. Technol.* 36, 73 (**2013**).

Received: 7 August 2017. Accepted: 6 September 2017.